# On Broadband Shock-Associated Noise Source and Radiation Characteristics from an Installed, Afterburning GE F404 Engine\*

Logan T. Mathews<sup>†</sup> and Kent L. Gee<sup>‡</sup>

Brigham Young University, Provo, UT, 84604, United States

Broadband shock-associated noise (BSN) is a major source of high-frequency noise in imperfectly expanded supersonic jets. While BSN has been extensively studied, source characterization from full-scale engines remains limited. This paper investigates BSN source and radiation characteristics from a full-scale, installed GE F404 engine on the T-7A trainer aircraft using acoustic holography. Apparent BSN sources are identified along the nozzle lipline and corroborated with in-situ imaging. The observed shock spacing aligns with similar jets in the literature but deviates significantly from traditional analytical models. Likewise, BSN peak frequencies at forward angles match trends from other full-scale jets but differ from simulations and lab-scale data, likely due to temperature and scale-related differences. A widely used BSN frequency model underperforms when relying on historical analytic shock spacing predictions but yields excellent agreement when corrected with measured spacing. Coherence analysis reveals connections between upstream-directed BSN and downstream Mach wave radiation, and shows elevated coherence between shock cells, indicating a partially coherent, distributed BSN source.

#### Nomenclature

 $A = \text{nozzle area, m}^2$ 

 $\beta_C$  = convergent nozzle off-design parameter equal to  $\sqrt{M_j^2 - 1}$ 

 $\beta$  = generalized off-design parameter equal to  $\sqrt{|M_j^2 - M_D^2|}$ 

D = nozzle, metersf = frequency, Hz

ratio of specific heats

 $L_n = n$ th shock cell spacing, measured as the distance between shock cell tips, meters

 $\overline{L}$  = average shock cell spacing/characteristic shock wavelength, meters  $\overline{L}_{\text{meas}}$  = average shock cell spacing from acoustical measurements, meters

M = Mach number

NPR = nozzle pressure ratio, defined as the ratio of the chamber pressure to the ambient pressure.

Sr = Strouhal number, defined as  $fD_i/U_i$ 

TTR = total temperature ratio, defined as the ratio of the inlet total temperature to the exit total temperature.

x = downstream distance from nozzle exit, meters
 y = sideline distance from jet centerline, meters

<sup>\*</sup> Distribution A: Approved for public release; distribution unlimited.

<sup>†</sup> PhD Candidate, Department of Physics and Astronomy, AIAA student member.

<sup>‡</sup> Professor, Department of Physics and Astronomy, AIAA Associate Fellow

#### Subscripts

a = ambient condition

c = relating to the convection (advection) of turbulence, wavepackets in the flow

conv = relating to a convergent nozzle

C-D = relating to a convergent-divergent nozzle

d = jet design conditione = exit jet condition

*j* = fully-expanded jet condition

t = throat jet condition

#### I. Introduction

In an imperfectly expanded supersonic jet, the mismatch between the nozzle exit pressure and ambient pressure gives rise to a series of oblique shocks and expansion fans. This structure forms a train of shock cells, commonly referred to as "Mach diamonds," which appear in the jet's potential core, as shown in Fig. 1. These shock structures interact with turbulent wavepacket-like structures in the shear layer, giving rise to two types of shock-associated noise [1]. The first type, known as screech, arises from a feedback loop between flow perturbations and the shock structure, resulting in discrete tonal components in the radiated sound [1-3]. Screech is most prominent in laboratory-scale and transonic jets, but has not been consistently observed in full-scale tactical aircraft engines[4]. The second type is broadband shock-associated noise (BBSAN or BSN), which has a broadband spectral character and typically radiates in the forward direction at frequencies higher than the dominant mixing noise.

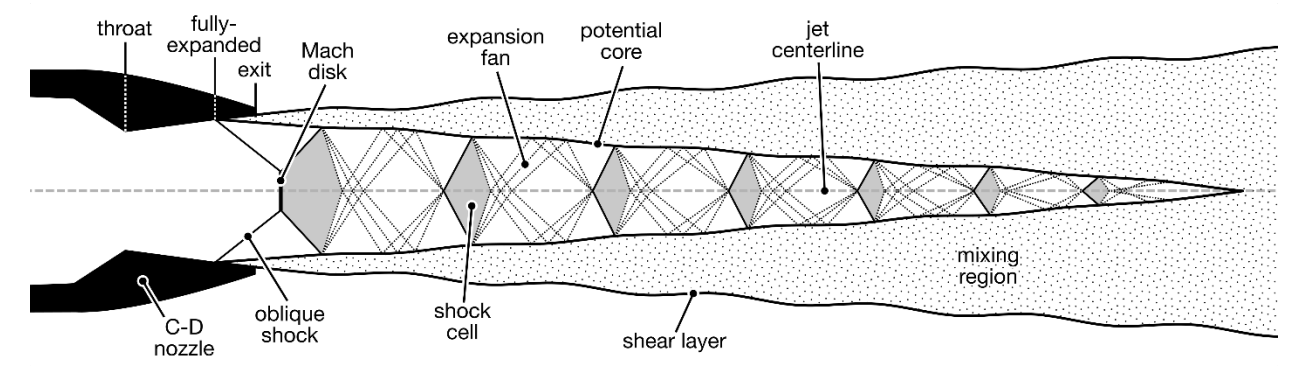


Figure 1. Schematic of shock structure in a supersonic, overexpanded jet.

The foundational study of BSN was conducted by Harper-Bourne and Fisher[1], who introduced a model for BSN in sonic jets from convergent nozzles. Their work, along with subsequent studies by Tanna[5] and Howe and Ffowcs-Williams[6], expanded the theoretical and experimental understanding of BSN from convergent nozzles. Further investigations extended this research to convergent-divergent (C-D) supersonic jets, notably by Seiner and Norum[4], Norum and Seiner[7,8], Pao and Seiner[9], and Seiner and Yu[10]. Important theoretical developments by Tam and Tanna[11], Tam et al. [12], and Tam[13] provided predictive models for BSN spectra and shock-cell structure. More recent studies—including experimental, numerical, and theoretical approaches—have broadened the scope of BSN research and increasingly connected fluid dynamic and acoustic domains [14-25].

Despite this progress, the direct characterization of BSN sources in full-scale, afterburning-capable engines remains limited, primarily due to the difficulty of capturing detailed in-situ flow measurements alongside acoustic data. These studies have primarily focused on acoustic characteristics radiated to the field [26,27,28]. Because of the constraints of full-scale measurements, most BSN studies have relied on unheated or mildly heated laboratory-scale jets or numerical simulations. While advances in computational modeling [29-32] and afterburning jet facilities [33,34] have improved understanding of highly heated jet acoustics, these approaches still require further validation against full-scale engine behavior.

This paper presents the most detailed source characterization of BSN in a full-scale, afterburning-capable jet engine to date. The apparent spatial characteristics of BSN sources are compared with in-situ photographs, and the apparent spacing of the noise sources and associated shock cells are compared with other models and data present in the literature. The peak frequency of the measured BSN as a function of radiation angle is compared to both analytical

models and data from other full-scale measurements. A coherence analysis is conducted of the radiated BSN, and coherence is found between upstream and downstream radiated noise from each apparent shock noise source, which suggests that upstream-radiated BSN may influence or couple with downstream-radiating mixing noise.

#### II. Methods

#### A. Measurement and Data

The data in this paper were obtained through an extensive acoustical measurement of the T-7A trainer aircraft in August 2019 at Holloman Air Force Base in New Mexico, USA. Additional details of this measurement campaign are given by Leete et al.[35]. This analysis uses a 120-element quasi-linear ground microphone array of ½" GRAS 46BD and 46BG pressure microphones located near the aircraft, depicted in Fig. 2. For context, the microphone array was located at its closest approximately 9 diameters from the centerline of the jet, and the peak BSN at the array was approximately 800-900 Hz, which translates to the closest microphones being in excess of 10 acoustic wavelengths away at these frequencies. The aircraft was run up through several engine conditions six times. This analysis uses the acoustic data averaged across the six engine runs at the maximum afterburner (AB) engine condition.

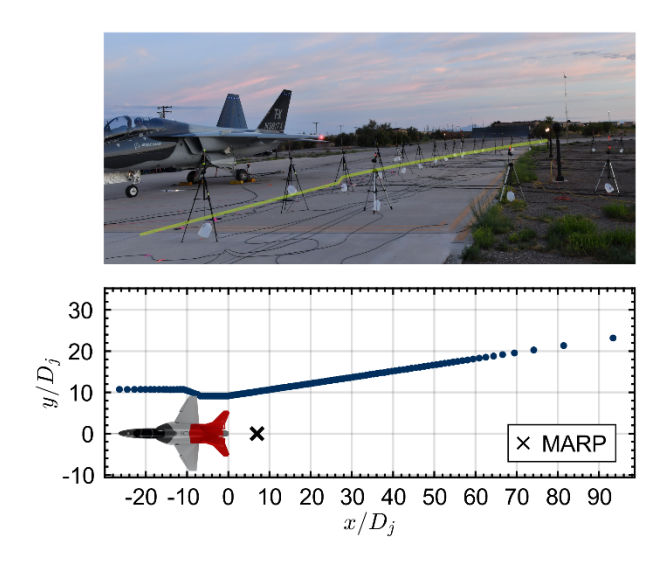


Figure 2. a) Photograph of aircraft as positioned during the measurement, microphone array highlighted in yellow. b) Schematic of microphone array, inlet angle shown.

Several key jet parameters for the T-7A at AB are reported in Table 1. These parameters were obtained through running a numerical propulsion system simulation code based on the ambient conditions of the test and input data from the engine during the run-ups. The jet was operating in an overexpanded condition at AB.

Table 1. Engine parameters at AB engine condition.

Parameter	Value
$M_j$	1.46
$M_d$	1.55
$eta_{ m conv}$	1.07
β	0.52

NPR	3.3	
TTR	7.0	

The design Mach number  $(M_d)$  for the nozzle is calculated from the transcendental quasi-1D area Mach number relation

$$\frac{A_e}{A_t} = \frac{1}{M_d} \left[ \frac{2}{\gamma + 1} \left( 1 + \frac{\gamma - 1}{2} M_d^2 \right) \right]^{\frac{\gamma + 1}{2(\gamma - 1)}},\tag{1}$$

where  $A_e$  is the exit area of the nozzle,  $A_t = A^*$  is the throat (critical) area of the nozzle, and  $\gamma$  is the ratio of specific heats[36].

The parameter  $\beta$  used in connection with BSN is an application of the Prandtl-Glauert factor. In the context of jet nozzle operation, it is often referred to as the off-design parameter and quantifies the degree to which a jet is operating off-condition. This parameter was first introduced in the jet noise literature by Harper-Bourne and Fisher[1] in the context of convergent nozzles and is defined as

$$\beta_{conv} = \sqrt{M_j^2 - 1},\tag{2}$$

where  $M_j$  is the fully-expanded Mach number of the jet. Though initially used for only convergent nozzles (hence the subscript conv used here for convenience), several subsequent studies used  $\beta_{conv}$  in their analysis of jets from both convergent and C-D nozzles (e.g. Refs. [4,7-10]). Hence, even though this parameter is not appropriate for the T-7A/F404, it is included here to compare with some of the historic literature that used it for C-D nozzles.

Tam and Tanna[11] introduced a slightly different, generalized formulation for  $\beta$  in the case of a C-D nozzle to achieve the same BSN intensity scaling of  $I_{\rm BSN} \propto \beta^4$ , which is given as

$$\beta = \sqrt{\left|M_j^2 - M_d^2\right|},\tag{3}$$

where  $M_d$  is the design Mach number of the nozzle. In the case of a convergent, choked nozzle,  $M_d = 1$ , hence the expression reduces to the same form as  $\beta_{\text{conv}}$ . Due to inconsistencies in the literature regarding the use of  $\beta$  and  $\beta_{\text{conv}}$ —particularly with several studies using  $\beta_{\text{conv}}$  to characterize C-D nozzles in supersonic flow—both parameters are reported here to facilitate comparison across the full range of existing research.

## **B.** Acoustical Holography

This paper leverages an acoustical holography-based analysis technique to reconstruct the acoustic field using the array microphone. This technique is discussed in mathematical detail in the context of this dataset by Mathews and Gee[37]. Other discussions of the holography method used are given in several papers[38,39]. The methods used in this paper are identical to those used in Ref. [37]. For the purposes of the discussion, a brief qualitative summary of the process is given here to orient the reader to the overall methodology of the process.

The statistically optimized near-field acoustical holography process begins with transforming the raw recorded pressure data from each array microphone into the frequency domain through traditional autospectral and crossspectral methods for noise. This results in a cross-spectral matrix at each frequency bin that contains both the magnitude and phase relationships between each microphone pair in the array. Given the partially coherent nature of jet noise, the spectral data from each frequency are then decomposed into individual partial fields using singular value decomposition, resulting in separate, self-coherent partial fields that can each have acoustical holography performed on them. Then, for each partial field at each frequency analyzed, the holographic algorithm is conducted: firstly, a numerical routine is employed to extend the aperture of the array and taper the ends of the array to zero amplitude to both prevent wraparound error, and to prevent errors from discontinuities present when the edges of the array are nonzero (similar in principle to the windowing required in Fourier analysis of noise). Then, a matrix of wavefunctions, referred to as an equivalent wave model (EWM), is constructed that contains analytic functions that form a basis for the acoustic field in a suitable geometry for the source in question. In the case of a jet, cylindrical wavefunctions are chosen and have been shown to be an appropriate choice [40]. Now, given the EWM and the measured pressures for the partial field at hand, a linear equation is formulated and the coefficients of the EWM are determined via a regularized pseudo-inverse, resulting in either a least-squares or minimum norm solution of coefficients, depending on the choice of dimensions for the EWM. In the case of this study, the system was set up to be underdetermined, and a minimum norm solution was sought. Finally, another similar matrix of wavefunctions is formulated, though the geometry of points to reconstruct can now be used in the wavefunctions, and the reconstructed field is estimated through the simple multiplications of the reconstruction EWM with the determined coefficients. Since each of the partial fields has its own EWM, the total result at each frequency is obtained by energetically summing the reconstructed partial fields.

## III. Analysis

#### A. Lipline Acoustic Reconstruction

To investigate the source characteristics of shock-associated noise, acoustic holography is employed to reconstruct the noise field along the nozzle lipline—an effective proxy for shock noise source locations. Because this reconstruction is based only on acoustic signals that reach the microphone array, it excludes near-field energy and hydrodynamic components. Therefore, the result represents only the portion of the acoustic field that successfully propagates to the array.

Figure 3 presents the reconstructed sound field along the nozzle lipline, shown as a function of downstream distance from the nozzle exit and frequency, expressed as the Strouhal number  $Sr = fD_j/U_j$ . Amplitude is color-mapped relative to the maximum value. A vertical white dashed line shows the estimated location of the potential core terminus. Below  $Sr \approx 0.35$ , the field is dominated by mixing noise, with at least three distinct local maxima. These features are discussed in detail by Mathews and Gee [37]. Above this threshold, however, vertical striations appear, continuing up to the upper frequency limit of the reconstruction at Sr = 0.5, highlighting their broadband character. Similar striations have been observed in both laboratory- and full-scale reconstructions [41,42], though with limited interpretation. In the present study, these features are further examined both spatially and spectrally, and evidence is presented linking them directly to shock noise sources.

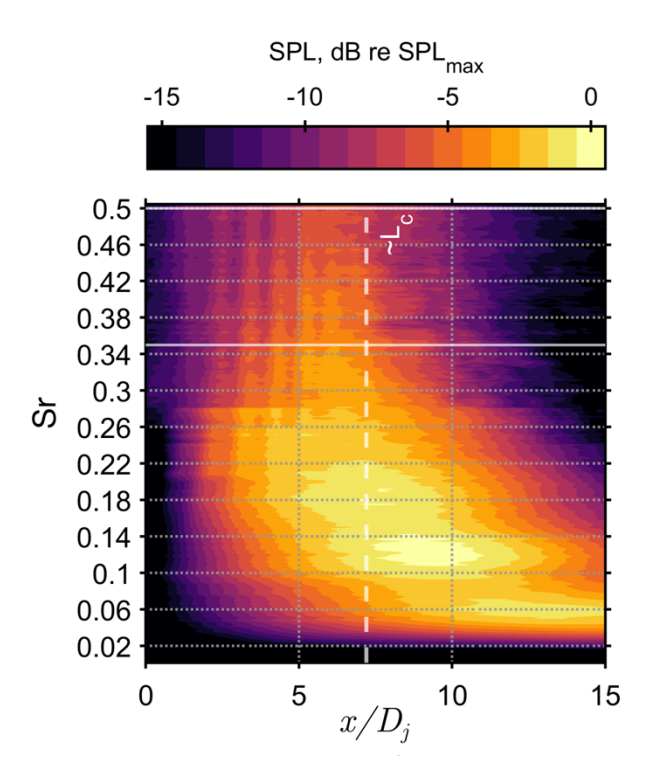


Figure 3. Spatiospectral acoustical holography reconstruction at the nozzle lipline. The estimated end of the potential core is indicated.

Since the shock noise sources are most prominent in the  $0.35 \le Sr \le 0.5$  region, and most of the mixing noise energy is below this band, this frequency band is selected as the analysis region for shock noise analyses in this paper. This region of analysis is indicated by the two horizontal white lines in Fig. 3.

To analyze the spatial characteristics of the noise sources, the reconstruction amplitude is integrated across this selected frequency range. The resulting spatial distribution is shown in Fig. 4. To reinforce the link between the observed acoustic sources and the shock cell structure, a scaled in-situ photograph of the jet is provided alongside the integrated acoustic reconstruction. Peaks in the reconstructed acoustic signature align with visible shock cell locations in the photograph, supporting the assertion that these noise sources are associated with shock-turbulence interactions.

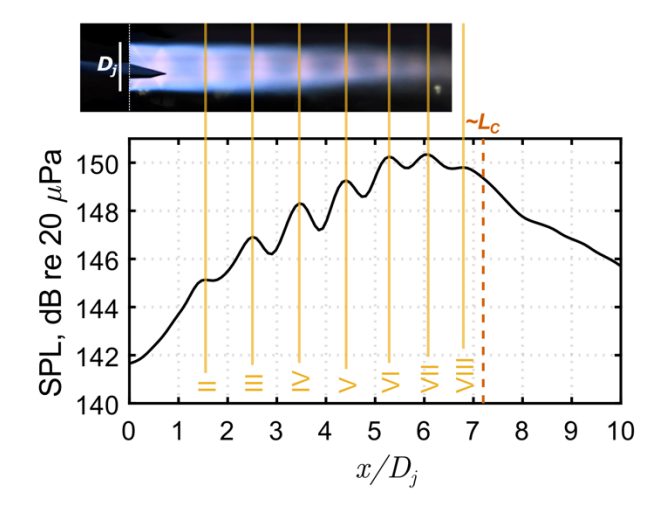


Figure 4. Integrated SPL from lipline holography reconstruction between  $0.35 \le Sr \le 0.5$  and comparison with in-situ scaled photograph of the jet at afterburner. Locations of suspected shock noise sources are indicated.

Remarkably, the first shock cell (I) does not correspond to a significant acoustic source in the reconstruction. This could indicate either a limitation in the measurement and reconstruction process or that the first shock cell radiates minimal acoustic energy. Harper-Bourne[43], using an acoustic mirror technique in a laboratory-scale jet, reported a similarly weak signature for the first shock cell. This may be attributed to the underdeveloped turbulence present near the nozzle exit upstream of the potential core terminus, which can be visually confirmed in many images of supersonic jets. The early work of Nagamatsu et al.[44] showed that sound power production in supersonic jets grows linearly downstream of the nozzle through the potential core region with very little sound power output in the first few jet diameters, and hence it would follow that less BSN would be radiated from the first few shocks. Interestingly, the amplitude of apparent BSN source locations in Fig. 4 grows roughly linearly through location VI, perhaps reflective of a linear increase in sound power output.

As shown in Fig. 4, the strongest acoustic signatures occur at shock locations VI and VII. This finding is consistent with results from Podboy et al.[45], who also observed that downstream shock cells produced the highest amplitude shock-associated noise.

These results reinforce the conclusion that radiated BSN in supersonic jets originates from discrete locations correlated with the shock cell structure, especially in the downstream portion of the potential core. The absence of strong radiation from the first shock cell suggests a dependence on turbulence development, highlighting the relationship between flow evolution and acoustic radiation. Overall, the holography analysis confirms that acoustically significant shock-turbulence interactions are spatially organized and spectrally broadband.

# **B. Shock Spacing**

Shock spacing in imperfectly expanded jets has long been studied due to its relevance to jet noise. The spacing between shocks has traditionally been linked to the peak frequency of the radiated noise and is often referred to as the "characteristic wavelength" of BSN. Several models have been proposed for this spacing, denoted as  $\overline{L}$ . One of the earliest analytical models is attributed to Pack [46], in what has come to be known as the Prandtl-Pack formula, given by

$$\frac{\bar{L}}{D_i} = \frac{\pi}{\mu_1} \sqrt{M_j^2 - 1} = 1.306 \,\beta_{conv} \tag{4}$$

where  $\mu_1$  is the first root of the zeroth-order Bessel function of the first kind  $(J_0(\mu_1) = 0)$ . This formula does not account for energy losses and is generally applicable only to the first shock, where such losses are minimal. To account for shock spacing reductions due to losses, Harper-Bourne and Fisher[1] introduced an empirical correction:

$$\frac{\overline{L}_n}{D_j} = 1.306 \,\beta_{conv} \left[ 1 - (n-1)\epsilon \right],\tag{5}$$

where  $\epsilon \approx 0.06$  is an empirical constant derived from experimental observations. Note that in the case of the first shock's spacing, Eq. (5) reduces simply to Eq. (4).

While this model was originally developed for convergent nozzles, it could potentially be generalized to use with C-D nozzles by substituting  $\beta$  for  $\beta_{conv}$ , leading to the expression

$$\frac{\bar{L}}{D_i} = \frac{\pi}{\mu_1} \beta = \sqrt{|M_j^2 - M_d^2|} = 1.306 \,\beta. \tag{6}$$

Figure 5 compares the inter-shock spacing estimated from the acoustical holography reconstruction with predictions from Eqs. (4–6) and measurements from other experimental and simulated jets. This includes overexpanded jet data from Norum and Seiner [8] and Podboy et al. [45], as well as LES results from Liu et al. for an underexpanded TTR = 7 jet [29] and an overexpanded TTR = 2.9 jet [30]. Notably, the latter jet closely matches the T-7A conditions, aside from the TTR. The spacing between shocks IV–VIII in that case shows excellent agreement with the acoustic estimates in this study. Given that the downstream shocks were identified as the most acoustically active, the best accuracy for acoustic identification of shock locations is expected here due to their higher signal-tonoise ratio.

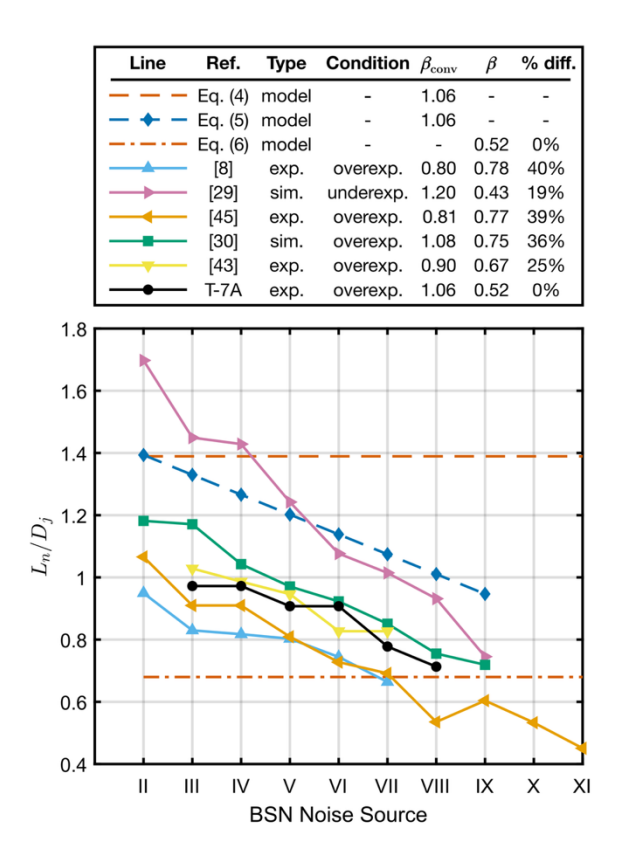


Figure 5. Inter-shock spacing for the jet in the present study compared with various models and other data sources in the literature. Details for each data source are given in the legend, including the data type (model, experiment, simulation), values of  $\beta_{conv}$  and  $\beta$ , as well as the percent difference between each value of  $\beta$  and that from the T-7A/F404 in this study.

Also noteworthy is that the underexpanded jet from Liu et al. [29], despite being a highly-heated supersonic F404-like jet with the closest  $\beta$  value among the comparisons, exhibits significantly larger shock spacing. Similar trends were observed in other underexpanded jets not shown here. While Eqs. (4) and (5) align well with the underexpanded jets, they fail to predict shock spacing for the overexpanded cases, likely due to their original design for convergent nozzles. Nevertheless, Eq. (5) agrees reasonably with  $L_{V-VIII}$  for the underexpanded jet in [29], even though it emanates from a C–D nozzle.

Furthermore, Eq. (6), which uses  $\beta$  instead of  $\beta_{conv}$ , does not reliably predict the average shock spacing for the jet in this study. The reason for this discrepancy is unclear but may stem from the limitations of using constants from convergent nozzle theory in C–D nozzle applications. This highlights the need for a more accurate, analytically derived model tailored to supersonic jets from C–D nozzles.

Also included in Fig. 5 are shock locations inferred from localized BSN sources by Harper-Bourne [43], using an acoustic mirror technique. Although that experiment used a cold, laboratory-scale model jet, the shock spacing results closely resemble those observed in this study. Both jets are overexpanded with similar  $\beta$  values. This similarity suggests that shock spacing—and hence the locations of BSN sources—is relatively insensitive to TTR and may be more directly correlated with  $\beta$  and whether the jet is over- or underexpanded.

Interestingly, when comparing the inferred shock locations from the T-7A/F404 with other datasets, the expansion condition appears to be the dominant factor influencing shock spacing, followed by  $\beta$ . The two datasets that showed the closest agreement were both overexpanded jets with the most similar values of  $\beta$ . However, even in these cases,  $\beta$  differed by as much as 36% from the T-7A/F404 value—highlighting that while  $\beta$  is a useful parameter, it alone may not fully capture the complexity of shock spacing behavior as appreciably large differences in  $\beta$  between different experiments gave similar results in terms of shock spacing.

In summary, shock cell spacing estimated from acoustical holography reveals limitations in current analytical models. While models such as the Prandtl–Pack relation and its variants provide reasonable predictions for underexpanded jets, they consistently fail to capture shock spacing in overexpanded flows from C–D nozzles. Notably, the trend of larger shock spacing in underexpanded jets compared to overexpanded ones is not reflected in existing formulations. These discrepancies highlight the need for updated models that accurately apply to C–D nozzles and span both over- and underexpanded regimes.

## C. Peak Frequency

Another key characteristic of BSN is its spectral peak frequency, which varies with angle—generally increasing as the observer moves downstream. Various models have been developed to describe this behavior, most of which build upon the formulation by Harper-Bourne and Fisher [1], which expresses the peak frequency as:

$$f_{pk}(\theta) = \frac{U_c}{\bar{L} (1 - M_c \cos \phi)'}$$
 (7)

where  $U_c$  is the convection velocity (typically taken as  $0.7U_j$ ),  $\bar{L}$  is the characteristic shock cell spacing,  $M_c$  is the convective Mach number, and  $\phi = 180^{\circ} - \theta$  is the angle relative to the jet axis. This model has been widely used in BSN studies [5,6,9]. In the present work, both the measured average shock spacing ( $\bar{L}_{meas}$ ) and the estimates from Eqs. (4) and (6) are used.

To identify BSN propagation angles, a shock noise reference point (SNRP) was selected based on the relative amplitudes of shock signatures in Fig. 4. Since signatures VI and VII exhibited the strongest amplitudes, the SNRP was placed between them at  $x/D_j = 5.6$  and this point was used as the origin from which to compute propagation angles. Figure 6(a) shows the SNRP location, several microphone positions, and their inlet angles relative to the SNRP. The corresponding autospectral densities are shown in Fig. 6(b), plotted against both frequency and Strouhal number. As expected, the BSN peak frequency increases with aftward angle, becoming most prominent between  $40^{\circ}$  and  $60^{\circ}$ .

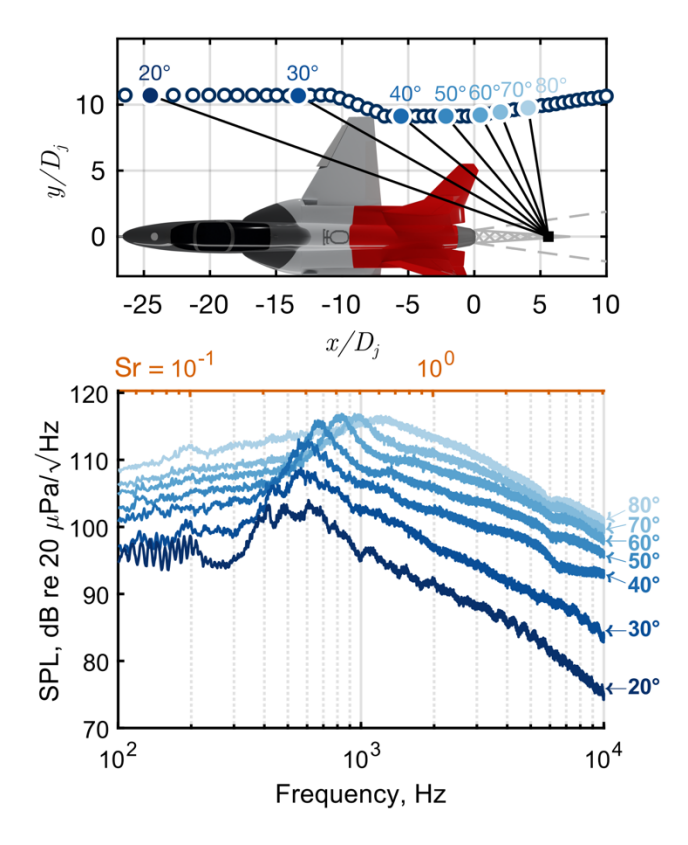


Figure 6. (a) Location of shock noise reference point and microphone locations for several angles. (b) Autospectral densities for each of the microphone locations indicated in (a).

To present a more comprehensive view of the BSN peak frequency angular variation, Figure 7(a) presents a spatiospectral map of SPL across the imaging array as a function of frequency and angle relative to the SNRP. The white line tracks the peak frequency trend. BSN dominates at angles below ~85°, while mixing noise prevails at angles >90°. Figure 7(b) isolates the peak frequency versus angle for clarity, and compares it with the model prediction from Eq. (6), evaluated using three different shock spacing estimates: one from Eq. (4), another from Eq. (6), and the  $\bar{L}_{\rm meas}$  as determined from Fig. 4 for the T-7A/F404 at AB. As expected, Eq. (4) performs poorly—consistent with its derivation for convergent nozzles and the mismatch shown in Fig. 5.

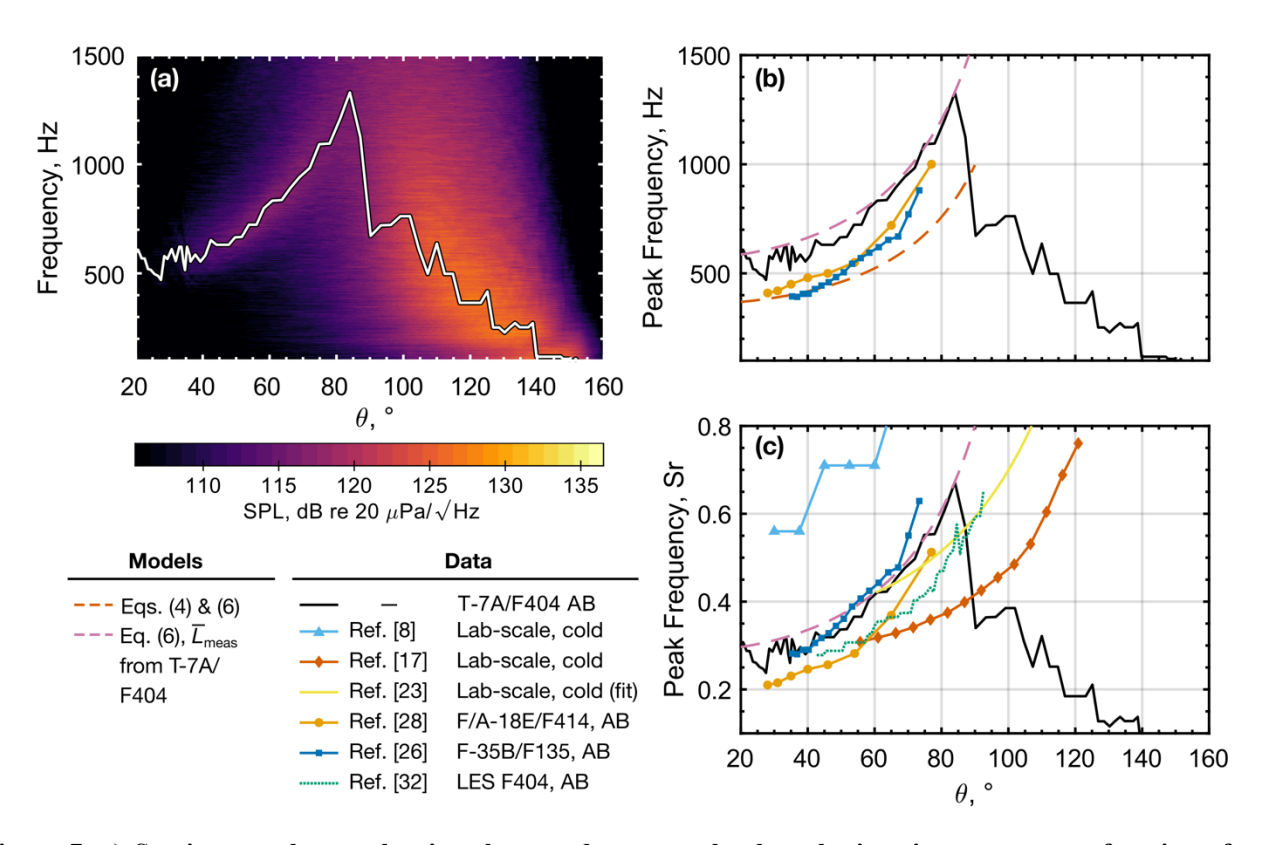


Figure 7. a) Spatiospectral map showing the sound pressure level at the imaging array, as a function of frequency and angle relative to the MARP. The peak frequency at each angle is shown by the white line. b) The peak frequency is depicted as a function of angle relative to the SCRP; additionally, two BSN peak frequency models are shown and two full-scale data sources are compared. c) The peak Strouhal number is shown as a function of angle relative to the SCRP, several datasets from the literature are also shown.

Additionally, Fig. 8(b) includes full-scale data from Refs. [26] and [28]. While trends are similar, the BSN peak frequencies measured here are consistently higher—by roughly half an octave—likely due to differences in jet diameter and velocity. To facilitate comparison across scales, Fig. 7(b) is recast in terms of Strouhal number in Fig. 7(c). Jet parameters from Refs. [26] and [28] were approximated for this conversion. For Ref. [26], values of  $U_j \approx 1400 \text{ m/s}$  and  $D_j \approx 1.0 \text{ m}$  were assumed. Ref. [28] lacked direct AB-condition parameters, but Seiner et al. [47] reported MIL-condition data for the same engine. A nominal 150% increase in  $U_j$  and  $D_j$  from MIL to AB yields approximate values of  $U_j \approx 1210 \text{ m/s}$  and  $D_j \approx 0.62 \text{ m}$ . While the trend from Ref. [26] aligns reasonably well, Ref. [28] reports lower Strouhal numbers, suggesting either physical differences or inaccuracies in parameter estimation.

Also shown in Fig. 7(c) are peak Strouhal number trends from several laboratory-scale jets [8,17,23]. These differ significantly from the T-7A and other full-scale results. The largest discrepancy is with Norum and Seiner [8], while data from Refs. [17] and [23] show moderate agreement but suggest more forward BSN radiation. One likely factor is temperature ratio: the lab-scale jets are cold, whereas the full-scale jets operate with afterburners. Kuo et al. [21] showed that for overexpanded jets, peak BSN frequency decreases with increasing TTR. Their data (up to TTR = 2.2) showed an 18% decrease in peak Strouhal number at 120° between TTR = 1 and TTR = 2.2. Given that AB operation corresponds to TTR  $\approx$  7, much lower peak Strouhal numbers are expected. Unfortunately, no afterburner-like lab-scale data are available in the open literature for direct comparison.

Lastly, Fig. 8(c) includes peak Strouhal trends from a large-eddy simulation of a TTR = 7 jet with an F404-like nozzle analyzed by Leete et al. [32]. While the LES results trend similarly to the T-7A data, their frequencies are generally lower, suggesting that while LES captures key features of afterburning BSN, further refinement is needed to match experimental results more closely.

## D. Coherence Analysis

Signal coherence is a valuable tool for assessing the linear relationship between two signals in the frequency domain. Coherence analyses have been employed by many recent jet noise studies to characterize various properties of jet noise[32,37,48-52]. In this study, coherence between the reconstructed sources at the nozzle lipline and microphones in the imaging array is used to investigate the source and propagation behavior of broadband shock-associated noise (BSN). Figure 8 shows coherence maps between each reconstructed source location at the lipline shock maxima (as identified in Fig. 4) and the field microphones. Each subfigure corresponds to a specific apparent source (II–VIII), and plots coherence ( $\gamma^2$ ) as a function of observer angle and Strouhal number. These maps provide insight into how energy from each apparent source radiates throughout the field.

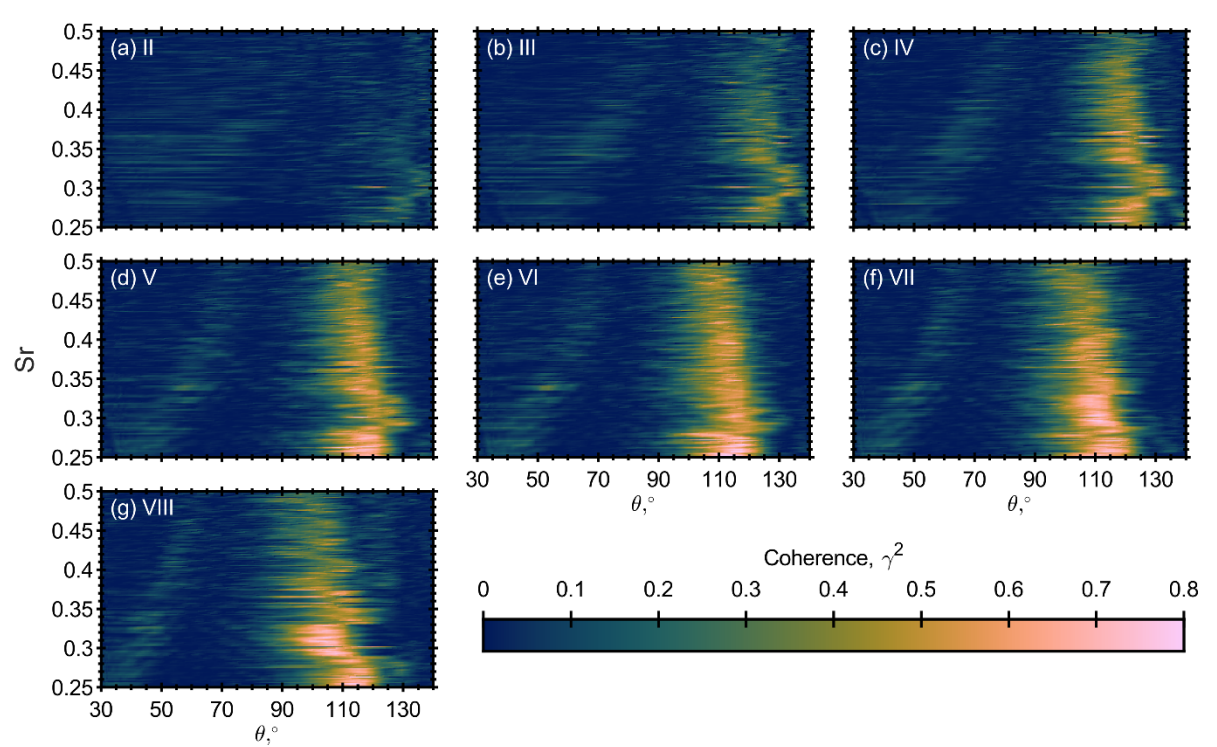


Figure 8. Coherence between each indicated shock locations at the nozzle lipline and imaging array microphones. Results are shown as a function of downstream distance as well as propagation angle relative to shock lipline location.

A few key trends are apparent. First, most apparent sources exhibit appreciable coherence with the field microphones over two distinct regions—aft (e.g., from 90-130°) and forward (e.g. 30-90°). This corresponds to the relative regions where mixing noise and BSN dominate, respectively as seen in Fig. 7(a). While the downstream angles have the greatest coherence with the apparent source locations, there is still moderate coherence levels at the upstream angles. This supports the idea that the turbulence interacting with the shock cells not only radiates Mach-wave-like energy downstream but also excites upstream-directed components. This supports similar findings by Swift et al.[51] at full-scale and Leete et al.[32] for a simulated, TTR = 7 jet.

Among the apparent sources, locations V-VIII exhibit the strongest and broadest coherence with the field, especially at mid-to-high angles. This suggests these sources contribute most prominently to the radiated BSN field and may correspond to the region of highest shock-turbulence interaction intensity. In contrast, sources II-IV show weaker coherence, particularly at higher Strouhal numbers, indicating their limited contribution to radiated BSN.

With coherence between the source region and the field established, further insight is gained by examining coherence within the source region itself. Figure 9 presents a coherence map computed between all pairs of lipline reconstruction locations—effectively a spatial correlation map along the nozzle lipline. Each axis corresponds to a location along the lipline (in diameters), and the color indicates the magnitude of coherence between source pairs.

Several key observations emerge from this map. First, location II again shows weak coherence with all other lipline locations, suggesting it may be acoustically isolated or that its contribution to the BSN mechanism is minimal. This aligns with the weak field coherence observed in Fig. 8(a). For sources III–VIII, however, a clear pattern of structured

coherence appears. The box-like shape and diagonal striations across the map reveal correlated activity between distinct shock locations.

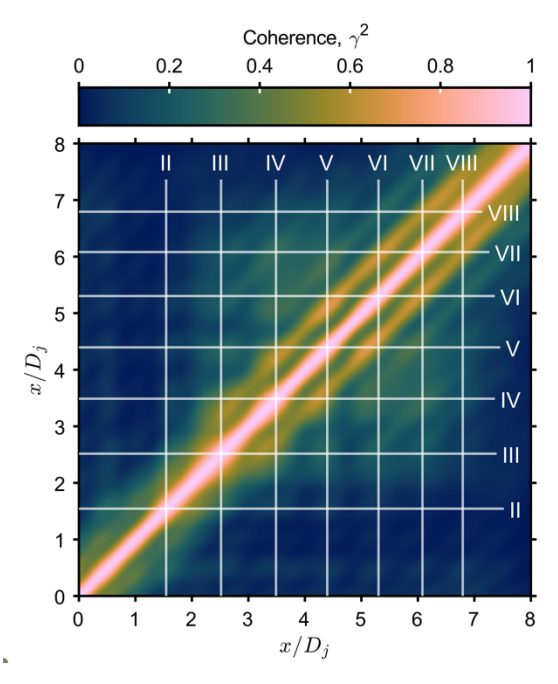


Figure 9. Coherence map along nozzle lipline with white grid lines indicating apparent shock noise source locations.

These off-diagonal coherence "islands" suggest that BSN generation is not purely localized but involves spatially distributed interactions—potentially due to the coherent advection of turbulence structures across multiple shock cells. For example, strong coherence between source III and sources IV–VII implies that a single turbulence structure/wavepacket may interact coherently with several consecutive shocks, radiating BSN at multiple spatial points. This fits with the findings of Seiner and Yu [10], who found appreciable spatial coherence spanning several shock wavelengths via correlations between near-field acoustic and flow sensors. Additionally, several recent wavepacket-based models for BSN include spatial coherence factors to appropriately model BSN [22,24].

In summary, the coherence analysis in Figs. 9 and 10 reveals that BSN generation is not confined to isolated points but is distributed and partially correlated across multiple shock cells. Certain locations, especially VI and VII, dominate the field radiation and share coherent links with other source regions. This supports the notion of a partially correlated BSN source mechanism, where turbulence structures interacting with successive shock cells generate spatially structured radiation. These findings emphasize the importance of modeling BSN as a distributed and interconnected source field, rather than as a sum of isolated monopoles.

## IV. CONCLUSION

Acoustic holography applied to a full-scale, installed F404 engine in afterburning overexpanded operation has revealed apparent sources of broadband shock-associated noise (BSN) along the nozzle lipline. These sources were identified solely from far-field microphone array measurements and show clear spatial correlation with shock structures visible in in-situ photographs of the jet in operation. The observed shock spacing matches closely with that seen in other similar overexpanded jets from the literature at both laboratory scale and in large-eddy simulations, yet two widely used analytical models—originally developed for convergent nozzles—fail to predict this spacing accurately. A possible generalization of the Prandtl—Pack model, replacing the off-design parameter with one adapted for convergent-divergent nozzles, also underperforms, highlighting the need for updated models that properly work for convergent-divergent nozzles and factor in whether the jet is under- or overexpanded.

Measured BSN peak frequencies show good agreement with other full-scale engine data when normalized by Strouhal number but diverge from laboratory-scale results—likely due to temperature differences, particularly the absence of afterburner heating in lab jets—but also possibly including other differences in the flow physics. The

Harper-Bourne and Fisher model for BSN peak frequency, when paired with analytic shock spacing estimates, fails to produce accurate BSN predictions for the F404/T-7A, however, substituting the measured average shock spacing yields excellent agreement. This underscores the potential for improved BSN modeling if shock spacing can be more accurately predicted.

Coherence analysis provides further insight into BSN radiation mechanisms. Apparent sources downstream—particularly BSN sources V-VII—exhibit strong coherence with the acoustic field downstream and moderate coherence upstream. Moreover, elevated coherence between multiple lipline shock locations suggests a spatially distributed, partially correlated source mechanism, wherein turbulence structures interact coherently with multiple shock cells. Overall, these findings reinforce the idea that BSN should be modeled not as a set of isolated monopole sources, but as a distributed and interconnected series of sources. Improved predictive models for shock spacing—specifically for C–D nozzles—could enhance both spectral and spatial predictions of BSN and inform jet noise reduction in future engine designs.

## **Funding Sources**

The authors acknowledge the Office of Naval Research for funding under grant number N00014-21-1-2069 with project monitor Steven Martens, Code 351 Jet Noise Reduction. The measurements were funded through the Advanced Pilot Training System Program Office and the Air Force Research Laboratory. This research was supported in part by the appointment of L. T. M. to the Department of Defense (DOD) Research Participation Program administered by the Oak Ridge Institute for Science and Education (ORISE) through an interagency agreement between the U.S. Department of Energy (DOE) and the DOD. ORISE is managed by Oak Ridge Associated Universities (ORAU) under DOE contract number DE-SC0014664. All opinions expressed in this paper are the authors' and do not necessarily reflect the policies and views of DOD, DOE, or ORAU/ORISE.

Professor Daniel Edgington-Mitchell of Monash University is thanked for his helpful discussion relating to this analysis.

#### References

<sup>&</sup>lt;sup>1</sup> Harper-Bourne, M., and Fisher, M. J., "The Noise from Shock Waves in Supersonic Jets," *Proc. AGARD Conf.*, Conference Preprint 131, September 1973.

<sup>&</sup>lt;sup>2</sup> Powell, A., "On the Mechanism of Choked Jet Noise," Proc. Phys. Soc. B 66(12), pp. 1039-1057 (1953). https://doi.org/10.1088/0370-1301/66/12/306

<sup>&</sup>lt;sup>3</sup> Yu, J. C., and Seiner, J. M., "Nearfield Observations of Tones Generated from Supersonic Jet Flows," ALAA 8th Aeroacoustics Conference, AIAA Paper 1983-0706, April 1983. https://doi.org/10.2514/6.1983-706

<sup>&</sup>lt;sup>4</sup> Seiner, J. M., and Norum, T. D., "Aerodynamic aspects of shock containing jet plumes," AIAA 6<sup>th</sup> Aeroacoustics Conference, AIAA Paper 1980-0965, June 1980. https://doi.org/10.2514/6.1980-965

<sup>&</sup>lt;sup>5</sup> Tanna, H. K., "An experimental study of jet noise part II: Shock associated noise," *Journal of Sound and Vibration* **50**(3), pp. 429-444 (1977). https://doi.org/10.1016/0022-460X(77)90494-1

<sup>&</sup>lt;sup>6</sup> Howe, M. S., and Ffowcs-Williams, J. E., "On the noise generated by an imperfectly expanded supersonic jet," Philosophical Transactions of the Royal Society of London. Series A, Mathematical and Physical Sciences 289(1358), pp. 271–314 (1978). http://doi.org/10.1098/rsta.1978.0061

Norum, T. D., and Seiner, J. M., "Broadband Shock Noise from Supersonic Jets," AIAA J. 20(1), pp. 68-73 (1982). https://doi.org/10.2514/3.51048

<sup>8</sup> Norum, T. D., and Seiner, J. M., "Measurements of Mean Static Pressure and Far-Field Acoustics of Shock-Containing Supersonic Jets," NASA TM-84521 (1982).

- <sup>9</sup> Pao, S. P., and Seimer, J. M., "Shock-Associated Noise in Supersonic Jets," ALAA J. 21(5), pp. 687-693 (1983). https://doi.org/10.2514/3.8134
- <sup>10</sup> Seiner, J. M., and Yu, J. C., "Acoustic Near-Field Properties Associated with Broadband Shock Noise," AIAA J. 22(9), pp. 1207-1215 (1984). https://doi.org/10.2514/3.8762
- <sup>11</sup> Tam, C. K. W., and Tanna, H. K., "Shock associated noise of supersonic jets from convergent-divergent nozzles," *Journal of Sound and Vibration* **81**(3), pp. 337-358 (1982). https://doi.org/10.1016/0022-460X(82)90244-9
- <sup>12</sup> Tam, C. K. W., Jackson, J. A., and Seiner, J. M., "A multiple-scales model of the shock-cell structure of imperfectly expanded supersonic jets," *Journal of Fluid Mechanics* 153, pp. 129-149 (1985). https://doi.org/10.1017/S0022112085001173
- <sup>13</sup> Tam, C. K. W., "Stochastic model theory of broadband shock associated noise from supersonic jets," *Journal of Sound and Vibration* 116(2), pp. 265-302 (1987). https://doi.org/10.1016/S0022-460X(87)81303-2
- <sup>14</sup> Lui, C., and Lele, S. K., "Sound Generation Mechanism of Shock-Associated Noise," 9th AIAA/CEAS Aeroacoustics Conference and Exhibit, AIAA Paper 2003-3315, May 2003. https://doi.org/10.2514/6.2003-3315
- <sup>15</sup> Long, D. F., "The Structure of Shock Cell Noise from Supersonic Jets," 11th AIAA/CEAS Aeroacoustics Conference, AIAA Paper 2005-2840, May 2005. https://doi.org/10.2514/6.2005-2840
- <sup>16</sup> Viswanathan, K., Alkislar, M. B., and Czech, M. J., "Characteristics of the Shock Noise Component of Jet Noise," AIAA J. 48(1), pp. 25-46 (2010). https://doi.org/10.2514/1.38521
- <sup>17</sup> Zaman, K. B. M. Q., Bridges, J. E., and Brown, C. A., "Excess Broadband Noise Observed with Overexpanded Jets," AIAA J. 48(1), pp. 202-214 (2010). https://doi.org/10.2514/1.43383
- <sup>18</sup> Miller, S. A. E., and Morris, P. J., "The prediction of broadband shock-associated noise including propagation effects," *International Journal of Aeroacoustics* **11**(7-8), pp. 755-781 (2012). https://doi.org/10.1260/1475-472X.11.7-8.75
- <sup>19</sup> André, B., Castelain, T., and Bailly, C., "Broadband Shock-Associated Noise in Screeching and Non-Screeching Underexpanded Supersonic Jets," AIAA J. 51(3), pp. 665-673 (2013). https://doi.org/10.2514/1.J052058
- <sup>20</sup> Liu, J., Corrigan, A., Kailasanath, K., Heeb, N., Munday, D., and Gutmark, E. (2013). "Computational Study of Shock-Associated Noise Characteristics Using LES," 19th AIAA/CEAS Aeroacoustics Conference, AIAA Paper 2013-2199, May 2013. https://doi.org/10.2514/6.2013-2199
- <sup>21</sup> Kuo, C. W., McLaughlin, D. K., Morris, P. J., and Viswanathan, K., "Effects of Jet Temperature on Broadband Shock-Associated Noise," *AIAA J.* **53**(6), pp. 1515-1530 (2015). https://doi.org/10.2514/1.J053442
- Wong, M. H., Jordan, P., Honnery, D. R., and Edgington-Mitchell, D., "Impact of coherence decay on wavepacket models for broadband shock-associated noise in supersonic jets," *Journal of Fluid Mechanics* 863, pp. 969-993 (2019). https://doi.org/10.1017/jfm.2018.984
- <sup>23</sup> Wong, M. H., Kirby, R., Jordan, P., and Edgington-Mitchell, D., "Azimuthal decomposition of the radiated noise from supersonic shock-containing jets," *Journal of the Acoustical Society of America* 148(4), pp. 2015-2027 (2020). https://doi.org/10.1121/10.0002166
- <sup>24</sup> Wong, M. H., Jordan, P., Maia, I. A., Cavalieri, A. V. G., Kirby, R., Fava, T. C. L, and Edgington-Mitchell, D., "Wavepacket modelling of broadband shock-associated noise in supersonic jets," *Journal of Fluid Mechanics* 918, A9 (2021). https://doi.org/10.1017/jfm.2021.324
- Nogueira, P. A. S., and Edgington-Mitchell, D., "Study of Broadband Shock-Associated Noise using the Parabolised Floquet Equations," 28th ALAA/CEAS Aeroacoustics Conference, AIAA Paper 2022-3063, June 2022. https://doi.org/10.2514/6.2022-3063
- <sup>26</sup> Vaughn, A. B., Neilsen, T. B., Gee, K. L., Wall, A. T., Downing, J. M., and James, M. M., "Broadband shock-associated noise from a high-performance military aircraft," *Journal of the Acoustical Society of America* 144, EL242 (2018). https://doi.org/10.1121/1.5055392

- <sup>27</sup> Aujogue, N., Huber, J., Julliard, E., Antoni, J., and Leclère, Q., "Experimental investigation of the supersonic jet noise from aircraft engines using acoustic imaging," 28th AIAA/CEAS Aeroacoustics 2022 Conference, AIAA Paper 2022-2867, Jun. 2022. https://doi.org/10.2514/6.2022-2867
- <sup>28</sup> Tam, C. K. W., Aubert, A. C., Spyropoulos, J. T., and Powers, R. W., "On the dominant noise components of tactical aircraft: Laboratory to full scale," *Journal of Sound and Vibration* 422, pp. 92-111 (2018). https://doi.org/10.1016/j.jsv.2018.02.023
- <sup>29</sup> Liu, J., Corrigan, A. T., Kailasanath, K., and Taylor, B. D., "Impact of the Specific Heat Ratio on the Noise Generation in a High-Temperature Supersonic Jet," 54th ALAA Aerospace Sciences Meeting, AIAA Paper 2016-2125, Jan. 2016. https://doi.org/10.2514/6.2016-2125
- Liu, J., and Ramamurti, R., "Numerical Study of Supersonic Jet Noise Emanating from an F404 Nozzle at Model Scale," AIAA SciTech Forum, AIAA Paper 2019-0807, Jan. 2019. https://doi.org/10.2514/6.2019-0807
- <sup>31</sup> Brès, G. A., Towne, A., and Lele, S. K., "Investigating the effects of temperature non-uniformity on supersonic jet noise with large-eddy simulation," 25th AIAA/CEAS Aeroacoustics Conference, AIAA Paper 2019-2730, May 2019. https://doi.org/10.2514/6.2019-2730
- <sup>32</sup> Leete, K. M., Gee, K. L., Liu, J., and Wall, A. T., "Coherence Analysis of the Noise from a Simulated Highly Heated Laboratory-Scale Jet," ALAA J. 58(8), pp. 3426-3435 (2020). https://doi.org/10.2514/1.J059112
- <sup>33</sup> Murray, N. E., Tinney, C. E., and Panickar, P., "Laboratory-Scale Afterburning Supersonic Jet Noise Reduction using Contoured Inserts," 28th AIAA/CEAS Aeroacoustics Conference, AIAA Paper 2022-3030, Jun. 2022. https://doi.org/10.2514/6.2022-3030
- <sup>34</sup> Kumar, A., Meadows, J., Olaveson, T. W., Gee, K. L., Mathews, L. T., and Pratt, H. J., "Far-field noise measurements of a supersonic jet operating near afterburning conditions," *Aerospace Science and Technology* 157, 109842 (2025). https://doi.org/10.1016/j.ast.2024.109842
- <sup>35</sup> Leete, K. M., Vaughn, A. B., Bassett, M. S., Rasband, R. D., Novakovich, D. J., Gee, K. L., Campbell, S. C., Mobley, F. S., and Wall, A. T., "Jet Noise Measurements of an Installed GE F404 Engine," AIAA SciTech Forum, AIAA Paper 2021-1638, Jan. 2021. https://doi.org/10.2514/6.2021-1638
- <sup>36</sup> Anderson, J. D., Modern Compressible Flow: With Historical Perspective, 4th ed., McGraw-Hill, New York, 2021.
- <sup>37</sup> Mathews, L. T., and Gee, K. L., "Acoustical Holography and Coherence-Based Noise Source Characterization of an Installed F404 Engine," *AIAA J.* **62**(6), pp. 2186-2199 (2024). https://doi.org/10.2514/1.J063543
- <sup>38</sup> Hald, J., "Basic Theory and Properties of Statistically Optimized Near-Field Acoustical Holography," *Journal of the Acoustical Society of America* 125(4), pp. 2105–2120 (2009). https://doi.org/10.1121/1.3079773
- <sup>39</sup> Wall, A. T., Gee, K. L., and Neilsen, T. B., "Multisource Statistically Optimized Near-Field Acoustical Holography," Journal of the Acoustical Society of America 137(2), pp. 963–975 (2015). https://doi.org/10.1121/1.4906585
- <sup>40</sup> Wall, A. T., Gee, K. L., Neilsen, T. B., McKinley, R. L., and James, M. M., "Military Jet Noise Source Imaging Using Multisource Statistically Optimized Near-Field Acoustical Holography," Journal of the Acoustical Society of America, 139(4), pp. 1938–1950 (2016). https://doi.org/10.1121/1.4945719
- <sup>41</sup> Leete, K. M., Wall, A. T., Gee, K. L., Neilsen, T. B., James, M. M., and Downing, J. M., "Acoustical Holography-Based Analysis of Spatiospectral Lobes in High-Performance Aircraft Jet Noise," AIAA J. 59(10), pp. 4166-4178 (2021). https://doi.org/10.2514/1.J059400
- <sup>42</sup> Morata, D., and Papamoschou, D., "High-Resolution Continuous-Scan Beamforming," AIAA J. 61(1), pp. 429-443 (2023). https://doi.org/10.2514/1.J061910
- <sup>43</sup> Harper-Bourne, M., "The Jet Noise of a Convergent-Divergent Nozzle," 28th AIAA/CEAS Aeroacoustics 2022 Conference, AIAA Paper 2022-2827, Jun. 2022. https://doi.org/10.2514/6.2022-2827
- <sup>44</sup> Nagamatsu, H. T., Sheer, R. E., and Horvay, G., "Supersonic Jet Noise Theory and Experiments," in Basic Aerodynamic Noise Research, NASA SP-207, July 1969.

- <sup>45</sup> Podboy, G. G., Wernet, M. P., Clem, M. M., and Fagan, A. F., "Noise Source Location and Flow Field Measurements on Supersonic Jets and Implications Regarding Broadband Shock Noise," NASA TM-2017-219544 (2017).
- <sup>46</sup> Pack, D. C., "A note on Prandtl's formula for the wavelength of a supersonic gas jet," Q. J. Mech. Appl. Math. **3**, pp. 173–181 (1950); doi.org/10.1093/qjmam/3.2.173.
- <sup>47</sup> Seiner, J. M., Jansen, B. J., and Ukeiley, L. S., "Acoustic Fly-Over Studies of F/A-18 E/F Aircraft During FCLP Mission," 9th AIAA/CEAS Aeroacoustics Conference, AIAA Paper 2003-3330, May 2003. https://doi.org/10.2514/6.2003-3330
- <sup>48</sup> Harker, B. M., Neilsen, T. B., Gee, K. L., Wall, A. T., and James, M. M., "Spatiotemporal-Correlation Analysis of Jet Noise from a High-Performance Military Aircraft," AIAA J. 54(5), pp. 1554-1566 (2016). https://doi.org/10.2514/1.J054442
- <sup>49</sup> Miller, S. A. E., "Broadband shock-associated noise near-field cross-spectra," Journal of Sound and Vibration 372, pp. 82-104 (2016). https://doi.org/10.1016/j.jsv.2016.01.048
- 50 Leete, K. M., Wall, A. T., Gee, K. L., Neilsen, T. B., Harker, B. M., and James, M. M., "Azimuthal coherence of the sound field in the vicinity of a high performance military aircraft," Proceedings of Meetings on Acoustics 29, 045007 (2016). https://doi.org/10.1121/2.0000673
- 51 Swift, S. H., Gee, K. L., Neilsen, T. B., Wall, A. T., Downing, J. M., and James, M. M., "Spatiotemporal-correlation analysis of jet noise from a round nozzle high-performance aircraft," 2018 AIAA/CEAS Aeroacoustics Conference, AIAA Paper 2018-3938, June 2018. https://doi.org/10.2514/6.2018-3938
- <sup>52</sup> Harker, B. M., Gee, K. L., Neilsen, T. B., Wall, A. T., and James, M. M., "Source characterization of full-scale tactical jet noise from phased-array measurements," Journal of the Acoustical Society of America 146(1), pp. 665-680 (2019). https://doi.org/10.1121/1.5118239